Electrochimica Acta 76 (2012) 8–15

Contents lists available at SciVerse ScienceDirect

Electrochimica Acta

journal homepage: www.elsevier.com/locate/electacta

Determination and modeling of the thermodynamic properties of liquid calcium–antimony alloys

Sophie Poizeau, Hojong Kim, Jocelyn M. Newhouse, Brian L. Spatocco, Donald R. Sadoway*

Department of Material Science and Engineering, Massachusetts Institute of Technology, Cambridge, MA 02139-4307, USA

ARTICLE INFO

Article history:
Received 5 January 2012
Received in revised form 3 April 2012
Accepted 3 April 2012
Available online 15 May 2012

Keywords:
Ca–Sb
Liquid alloy
Thermodynamic properties
Association model
Molecular interaction volume model

ABSTRACT

The thermodynamic properties of Ca–Sb alloys were determined by emf measurements in a cell configured as Ca(s)|CaF_2|Ca–Sb over the temperature range 550–830 °C. Activity coefficients of Ca and Sb, enthalpy, Gibbs free energy, and entropy of mixing of Ca–Sb alloys were calculated for $x_{Ca} < 0.55$. To explain the connection between short-range order of liquid Ca–Sb alloys and the strong deviation from ideality in the thermodynamic properties, two thermodynamic models were invoked and reconciled: the regular associated solution model, assuming the presence of a $CaSb_2$ associate, and the molecular interaction volume model (MIVM). For the first time, the MIVM was used successfully to model the activity coefficients of a system with high-melting intermetallics, reducing the number of fitting parameters necessary from 5 (regular associated model) to 2 (MIVM). From the interaction parameters optimized by fitting at 800 °C, the activity coefficient of Ca was predicted at 650 °C, with an average error of less than 0.6% in the emf value.

1. Introduction

The interest in calcium-semimetal liquid alloys has grown with the recent developments in liquid metal batteries [1]. In a Ca-based liquid metal battery, the calcium from the negative electrode alloys with the semimetal in the positive electrode during discharge. The driving force for the alloying reaction is the difference in chemical potential between pure Ca and Ca alloyed with the semimetal. Knowledge of the variation of the calcium activity in the alloy enables one to calculate the theoretical voltage of such a battery, i.e. the theoretical discharge curve.

Previously, Delcet et al. [2] measured the properties of mixing of calcium in Ca–Sb alloys at 800 °C for $x_{Ca} < 0.5$. Delcet titrated Ca from a large Ca–Bi reference electrode ($x_{Ca} = 0.1$) through a single crystal CaF_2 electrolyte to a Ca–Sb working electrode and measured the emf. Delcet used a Ca-Bi reference electrode to depress the activity of Ca and prevent its solubility in the electrolyte. No secondary reference electrode was mentioned in the set-up. The container used for the Ca–Sb electrode was tungsten, which does not alloy with Sb or Ca. Delcet reported the activity coefficient of Ca in Ca–Sb alloys for $x_{Ca} = 0.1$, 0.2, 0.3, 0.4, and 0.5.

Bouhajib et al. [3] used a drop calorimetry method to determine the enthalpy of formation of Ca–Sb alloys at 805 °C for $0.04 < x_{Ca} < 0.6$. He also reported the enthalpy of formation of alloys at 704 and 750 °C for $x_{Ca} = 0.1$ and 0.2. Bouhajib calibrated the Calvet calorimeter under flowing argon by dropping room temperature Sb shots. The container of the Sb bath was not mentioned. Ca samples were weighed in a glove box and added to the Sb bath. Bouhajib measured the partial enthalpy of mixing of Ca and the enthalpy of formation of Ca–Sb alloys, but only the latter are reported in [4]. There is a disparity between these results and those found earlier by Delcet, which Bouhajib acknowledges [5]: Bouhajib obtained at 805 °C −119 and −129 kJ/mol for the partial Gibbs energy of Ca for $x_{Ca} = 0.1$ and 0.2, respectively, while Delcet had obtained −185 and −195 kJ/mol for the same compositions at 800 °C.

Given the large discrepancy between the two sets of results, the first objective of this study was to make an accurate determination of the properties of mixing of Ca–Sb liquid alloys between 550 and 830 °C for $0.01 < x_{Ca} < 0.95$. The second objective was to interpret the results for the liquid alloys using two thermodynamic models: the association model [6], the accepted model of reference for systems with high melting intermetallics, and the molecular interaction volume model (MIVM) [7], never used for such systems (i.e. forming high-melting intermetallics). The main difference between these models is that the associate model assumes the existence of an associate species Ca_xSb_y in the liquid alloy while the MIVM does not. This study attempts to reconcile these different modeling approaches in the case of Ca–Sb.

The thermodynamic properties of Ca–Sb alloys were determined in this work by emf measurements, where the composition of each Ca–Sb alloy was kept constant, while the temperature was varied. A similar method has been used in the past by a variety of authors, such as Tamaki et al. [8] in the case of Na–Sn liquid alloys,

* Corresponding author. Tel.: +1 6172533487.

0013-4686/$ – see front matter © 2012 Elsevier Ltd. All rights reserved.
http://dx.doi.org/10.1016/j.electacta.2012.04.139

using a Na β-alumina solid electrolyte, or Petric et al. [9] in the case of K–Bi using a K β-alumina solid electrolyte. The electrolyte chosen in this study is CaF_2, as in the coulometric titration by Delcet et al. [2]. However, unlike a coulometric titration, the emf method used in this study does not require the passage of current, allowing the electrolyte to be sufficiently thick to suppress electronic conduction even when using Ca(s) as a reference electrode.

2. Experimental procedure

The experimental set-up used in the present work is similar to that used by Kim et al. [10], but was adapted to the alloys studied here.

2.1. Preparation of the alloys and electrolyte

The preparation of the sintered CaF_2 electrolyte is described in [10]. In a similar manner, CaF_2 caps were prepared and served to mitigate the evaporation of the alloys, and in particular of the more volatile Sb.

For most alloys, the calcium (99.99% metals basis, Sigma Aldrich, Stock No. 441872) and the antimony (99.999% metals basis, Alfa Aesar, Stock No. 11348) were weighed out in the glovebox, then arc melted using a MAM1 (Edmund Bühler GmbH). Due to the high volatility of the antimony, the alloys were weighed after arc melting to check that the evaporation was minimal (equivalent to less than 1 at% change in concentration). These samples were machined into cylinders 3–5 mm high and 9 mm in diameter, and a hole was drilled to accommodate the tungsten electrode lead.

For the alloys with high melting points ($Ca_{11}Sb_{10}$ + Ca_5Sb_3 and Ca_5Sb_3 + $CaSb_2$ regions), arc melted samples were inhomogeneous, porous, and fragile, resulting in poor contact to electrical leads. For this reason, samples for x_{Ca} = 0.55 and 0.63 were prepared by a powder processing method, adapted from Zevalkink et al. [11]. For these samples, pure metals were weighed out in an Ar-filled glovebox, ball milled for 1 h in stainless steel crucibles and steel ball milling media, uniaxially hot pressed at 40 MPa under Ar gas at 800 °C for 4 h (x_{Ca} = 0.55) or at 1600 °C for 12 h (x_{Ca} = 0.63), and then annealed for 72 h under vacuum at 650 °C (x_{Ca} = 0.55) or 400 °C (x_{Ca} = 0.63). These samples were prepared in the shape of cylinders 3–5 mm high and 12 mm in diameter. A tungsten rod of 3 mm in diameter was used for a compression contact to provide a larger contact area for these samples that remained solid throughout the experiment.

2.2. Set-up

The experiment is run under ultra-high purity argon (99.999%) in a closed crucible described previously [10]. A schematic of the electrochemical cell is presented in Fig. 1. Six wells were machined into the CaF_2 electrolyte pellet to contain 2 reference electrodes (RE) and 4 working electrodes (WE), the latter consisting of the Ca–Sb alloys of interest. An additional well is present in the center for a thermocouple. The reference electrodes were either pure Ca or a Ca–Sb alloy (x_{Ca} = 0.40) in the two phase region liquid + $Ca_{11}Sb_{10}$ throughout the emf measurements. The CaF_2 caps were positioned above the samples and proved to be effective in reducing the evaporation of the alloys.

2.3. Emf measurements

The air tight crucible was assembled inside an ultra-high purity Ar-filled glove box (O_2 concentration < 1 ppm) and kept under active vacuum (~1 Pa) for 12 h at 120 °C. Except for the high-melting samples (x_{Ca} = 0.55 or 0.63), the experiment was started at a temperature above the melting point of the electrodes to ensure good contact with the tungsten electrical leads and the electrolyte. Samples were then cooled to 600 °C or less (depending on composition) in increments of 40–20 °C, dwell time at each step ~90 min, and heated back up to 800 °C by intermediate steps. All temperature changes were made with a 5 °C/min ramp rate. The duration of the experiment was less than 24 h.

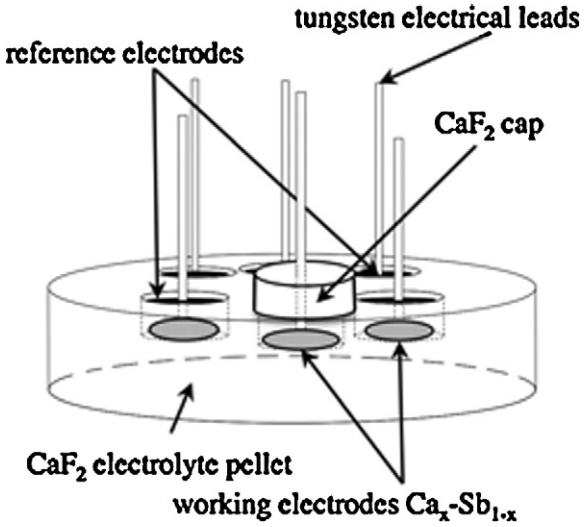

Fig. 1. Electrochemical cell.

The emf between one of the REs and the other electrodes was measured using a potentiostat-galvanostat (Autolab PGSTAT 302N, Metrohm AG), and the temperature was measured simultaneously using an ASTM type-K thermocouple. For the analysis of the results, the emf data considered were those recorded after the temperature reached a constant value (standard deviation < 0.5 °C). For all-liquid and partially liquid alloys, the thermodynamic equilibrium was reached almost immediately, while for alloys in a solid + solid 2-phase region, the thermodynamic equilibrium was reached up to 30 min after temperature equilibration. At each temperature step, the alloys were held at thermodynamic equilibrium for more than 30 min.

3. Results and data analysis

The overall cell reaction is the alloying of calcium in antimony according to the following two steps, which correspond to the half reactions at the electrodes:

$$\text{RE} : Ca_{(s)} = Ca^{2+} + 2e^-$$

$$\text{WE} : Ca^{2+} + 2e^- = Ca_{\text{in Sb}}$$

In some instances, the reference electrode was pure calcium, while in others a Ca–Sb alloy of fixed composition (x_{Ca} = 0.40) and known Ca activity served this purpose. All data reported herein have been expressed in terms of the pure calcium reference electrode. The variation of emf with temperature is plotted in Fig. 2. The alignment of the datapoints upon heating and cooling and between different experiments (for instance in the case of x_{Ca} = 0.10), attests to the reversibility and reproducibility of these measurements. In addition, the difference between the two reference electrodes was less than 2 mV. The datapoints obtained for Ca-rich alloys (x_{Ca} > 0.625) were not reproducible enough to be used in the derivation of the thermodynamic properties of mixing. Indeed, the error in emf was almost as high as the values themselves (less than 10 mV) for x_{Ca} > 0.80. The data for x_{Ca} = 0.63 were irreproducible (possibly due to oxidation during the experiment).

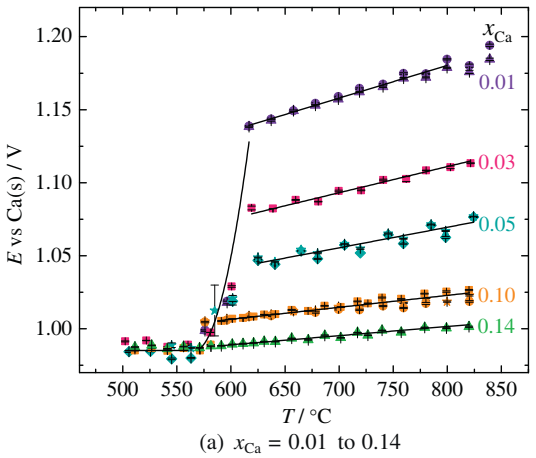

(a) x_{Ca} = 0.01 to 0.14

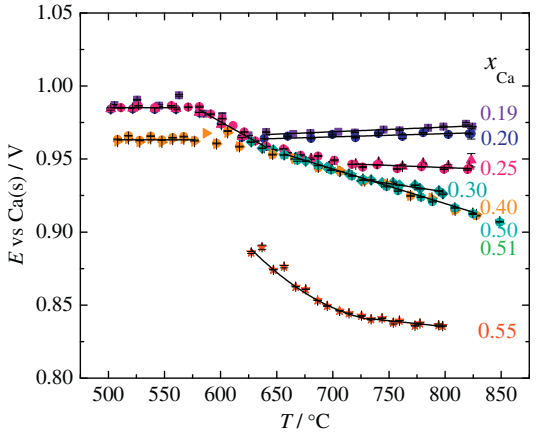

(b) x_{Ca} = 0.19 to 0.55

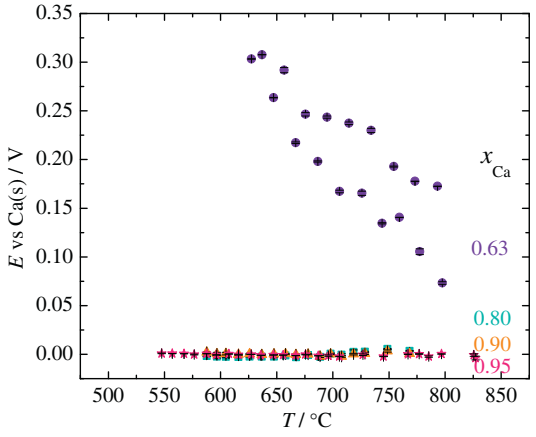

(c) x_{Ca} = 0.63 to 0.95

Fig. 2. Emf vs. temperature data for Ca(s)|CaF_2|Ca–Sb cells between 500 °C and 830 °C.

Fig. 3 presents the isothermal variation of emf at 700 °C with increasing Ca content. The data were extracted from the measurements at constant Ca concentration presented in Fig. 2 and show a major drop in the emf value (about 0.6 V) from the low Ca to high Ca sides of Ca_5Sb_3. This is consistent with the qualitative observation that samples with $x_{Ca} > 0.625$ oxidize much faster than those at lower Ca concentrations, indicating a large increase in Ca activity, which corresponds to a much lower emf.

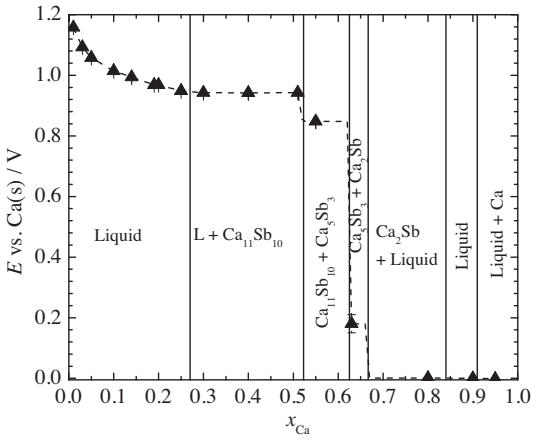

Fig. 3. Emf vs. Ca concentration in Ca–Sb alloy for Ca(s)|CaF_2|Ca–Sb cells at 700 °C.

3.1. Data analysis

The emf E measured between the reference and working electrode can be expressed by the Nernst equation:

$$E_{RE} = E^0_{Ca} + \frac{RT}{2F} \ln a_{Ca^{2+}} \quad (1)$$

$$E_{WE} = E^0_{Ca} + \frac{RT}{2F} \ln \left(\frac{a_{Ca^{2+}}}{a_{Ca}} \right) \quad (2)$$

$$E = E_{WE} - E_{RE} = -\frac{RT}{2F} \ln a_{Ca} \quad (3)$$

where E^0_{Ca} is the standard potential of pure calcium at the temperature T (in K), and R and F are the gas constant and the Faraday constant respectively. The activity of Ca^{2+} in the electrolyte, $a_{Ca^{2+}}$, is the same in Eqs. (1) and (2). The activity of Ca in the Ca–Sb alloy is noted a_{Ca}. It is the only unknown and can be directly calculated from the emf.

The activity of the calcium, a_{Ca}, can be related to the partial Gibbs free energy of calcium, $\Delta\overline{G}_{Ca}$, by $\Delta\overline{G}_{Ca} = RT \ln(a_{Ca})$. The results for the partial Gibbs free energy of calcium at 800 °C are presented in Fig. 4 along with the results from the literature reported by Delcet et al. [2] and Bouhajib et al. [5]. The results obtained in this work are consistent with those of Delcet.

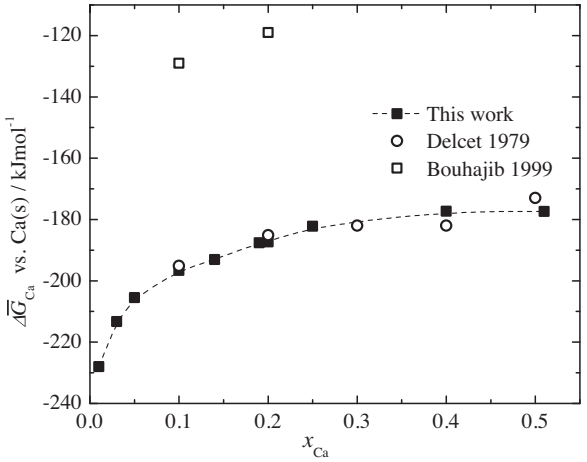

Fig. 4. Partial molar Gibbs free energy vs. Ca concentration in Ca–Sb alloys at 800 °C.

3.2. Activity coefficients and thermodynamic properties of mixing

The activity coefficient of antimony and the integral thermodynamic properties of mixing, the Gibbs free energy, ΔG, the entropy, ΔS, and the enthalpy, ΔH, were derived according to the integral Gibbs–Duhem relationships:

$$\ln \gamma_{Sb} = -x_{Ca}(1 - x_{Ca})\alpha(x_{Ca}) - \int_0^{x_{Ca}} \alpha(c)\,dc \quad (4)$$

$$\Delta G = (1 - x_{Ca}) \int_0^{x_{Ca}} \alpha(c)\,dc \quad (5)$$

$$\Delta S = (1 - x_{Ca}) \int_0^{x_{Ca}} \beta(c)\,dc \quad (6)$$

$$\Delta H = \Delta G + T\Delta S \quad (7)$$

where

$$\alpha(x_{Ca}) = \frac{\Delta \overline{G}_{Ca}}{(1 - x_{Ca})^2} \quad (8)$$

$$\beta(x_{Ca}) = -\frac{(\partial \Delta \overline{G}_{Ca}/\partial T)_{x_{Ca}}}{(1 - x_{Ca})^2} \quad (9)$$

and x_{Ca} is the mole fraction of calcium in the alloy.

$\Delta \overline{G}_{Ca}(x_{Ca}, T)$ was fitted as a linear function of temperature for constant composition, giving $\Delta \overline{H}_{Ca}(x_{Ca}, T)$ and $\Delta \overline{S}_{Ca}(x_{Ca}, T)$ by the relation $\Delta \overline{G}_{Ca}(x_{Ca}, T) = \Delta \overline{H}_{Ca}(x_{Ca}, T) - T\Delta \overline{S}_{Ca}(x_{Ca}, T)$ in the all-liquid region, in the liquid + $Ca_{11}Sb_{10}$ region, and in the $Ca_{11}Sb_{10}$ + Ca_5Sb_3 region (Table 1). In the low temperature solid + solid regions (Sb + $CaSb_2$ and $CaSb_2$ + $Ca_{11}Sb_{10}$ regions), $\Delta \overline{G}_{Ca}$ was found to be independent of temperature. In the L + Sb and low temperature $Ca_{11}Sb_{10}$ + Ca_5Sb_3 regions, the emf did not vary linearly with temperature and was found to follow $E = a + bT + cT\ln(T)$, with T in K (Table 2). The same fit was used by Petric et al. [9] in the case of K–Bi alloys.

$\alpha(x_{Ca})$ and $\beta(x_{Ca})$ were then fitted with a piecewise cubic hermite interpolating polynomial before the integration to obtain a_{Sb}, ΔG, ΔS and ΔH. The results at 800 °C are presented in Fig. 5, with the data in Table 3. a_{Ca} and a_{Sb} are reported with reference to Ca(s) and Sb(l), while the thermodynamic properties of mixing are reported with reference to Sb(l) and undercooled Ca(l). In the 2-phase regions, the chemical potentials of Ca and Sb do not change with composition; therefore, the integral properties of mixing vary linearly with composition at a given temperature. The equations for $\Delta H(x_{Ca})$ and $\Delta S(x_{Ca})$ in these regions are reported in Table 3, as well as their values for $Ca_{11}Sb_{10}$ and Ca_5Sb_3.

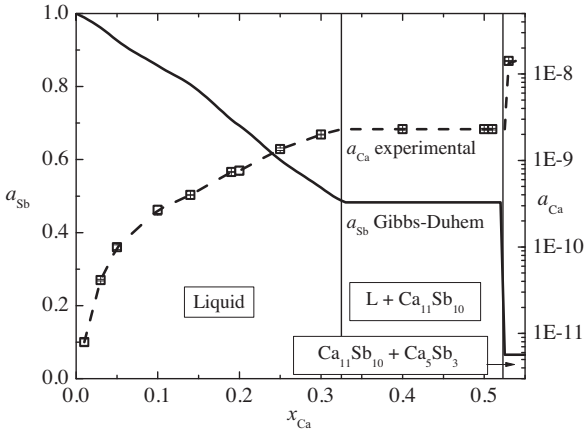

Fig. 5. Activities of Ca and Sb vs. Ca concentration in Ca–Sb alloys at 800 °C (data in Table 3).

3.3. Phase diagram

From the intersection points of the emf fitting lines, the liquidus temperatures of the Ca–Sb alloys as well as the eutectic and peritectic temperatures can be extracted for $x_{Ca} < 0.5$. When an alloy, for instance $x_{Ca} = 0.05$, undergoes a first-order phase transition, e.g. from a liquid phase to a L + Sb phase, it exhibits a discontinuity in the first derivative of the free energy with respect to temperature: i.e. the free energy varies continuously with temperature, but undergoes a slope change at the transition temperature. This slope change corresponds to the entropy of melting. Since the Gibbs free energy of the alloy is the weighted sum of the partial Gibbs free energies of each component, those partial free energies, and therefore the emf, undergo a slope change at the melting temperature as well. From Tables 1 and 2, the fit for the emf signal can be extracted for the samples at different temperatures. By finding numerically the

Table 1
Partial molar enthalpy and entropy of calcium in Ca–Sb alloys vs. Ca(s) determined from the linear fit of the experimental data (T in K), with the temperature range over which the fit is valid.

x_{Ca}	T (°C)	$\Delta \overline{H}_{Ca}$ (kJ/mol)	$\Delta \overline{S}_{Ca}$ (J/mol/K)
0.01	616–800	−181 ± 1	43 ± 1
0.03	619–822	−177 ± 1	35 ± 1
0.05	624–825	−177 ± 2	27 ± 2
0.10	591–821	−180.4 ± 0.5	15.8 ± 0.6
0.14	591–821	−180.3 ± 0.6	12.1 ± 0.6
0.19	640–825	−181 ± 1	6.2 ± 0.9
0.20	638–824	−182 ± 1	4 ± 1
0.25	720–824	−188 ± 2	−6 ± 2
0.30	726–798	−202 ± 2	−22 ± 2
L + $Ca_{11}Sb_{10}$	666–828	−226.6 ± 0.7	−45.8 ± 0.7
L + $CaSb_2$	580–641	−261 ± 4	−83 ± 4
$Ca_{11}Sb_{10}$ + Ca_5Sb_3 high T	734–798	−178 ± 3	−15 ± 3
Sb + $CaSb_2$	502–580	−190.10 ± 0.02	0
$CaSb_2$ + $Ca_{11}Sb_{10}$	508–577	−185.9 ± 0.1	0

Table 2
Emf (in V) measured vs. Ca(s) as a function of temperature (in K) non-linear fits: $E = a + bT + cT\ln(T)$.

x_{Ca}	T (°C)	a	b	c
L + Sb	571–617	82 ± 8	−0.75 ± 0.07	0.097 ± 0.009
$Ca_{11}Sb_{10}$ + Ca_5Sb_3 low T	627–734	9 ± 2	−0.07 ± 0.01	0.008 ± 0.002

Table 3
Activities of Ca and Sb vs. Ca(s) and Sb(l), and enthalpy and entropy of mixing vs. Ca(l) and Sb(l) at 800 °C.

x_{Ca}	a_{Ca}	a_{Sb}	ΔH (kJ/mol)	ΔS (J/mol/K)
0.01	8.15×10^{-12}	0.989	−1.97	0.380
0.02	1.97×10^{-11}	0.976	−3.85	0.713
0.04	6.06×10^{-11}	0.944	−7.56	1.25
0.06	1.19×10^{-10}	0.910	−11.3	1.63
0.08	1.81×10^{-10}	0.883	−15.0	1.89
0.10	2.46×10^{-10}	0.857	−18.8	2.06
0.12	3.11×10^{-10}	0.832	−22.6	2.17
0.14	3.90×10^{-10}	0.806	−26.4	2.24
0.16	5.12×10^{-10}	0.770	−30.1	2.27
0.18	6.65×10^{-10}	0.729	−33.9	2.25
0.20	8.16×10^{-10}	0.693	−37.7	2.15
0.22	1.01×10^{-9}	0.657	−41.5	1.96
0.24	$1.24 \times 10^{-\times 10^{-6}}$	0.617	−45.5	1.68
0.26	1.46×10^{-9}	0.583	−49.5	1.28
0.28	1.69×10^{-9}	0.553	−53.6	0.74
0.30	1.93×10^{-9}	0.523	−57.8	0.0122
0.32	2.30×10^{-9}	0.493	−62.4	−1.08
$Ca_{11}Sb_{10}$	2.23×10^{-9}	0.483	−114	−16.8
Ca_5Sb_3	1.43×10^{-8}	0.0654	−130	−18.5
L + $Ca_{11}Sb_{10}$	2.23×10^{-9}	0.483	$18.8 - 254x_{Ca}$	$23.6 - 77.1x_{Ca}$
$Ca_{11}Sb_{10}$ + Ca_5Sb_3	1.43×10^{-8}	0.0654	$-32.3 - 156x_{Ca}$	$-7.46 - 17.6x_{Ca}$

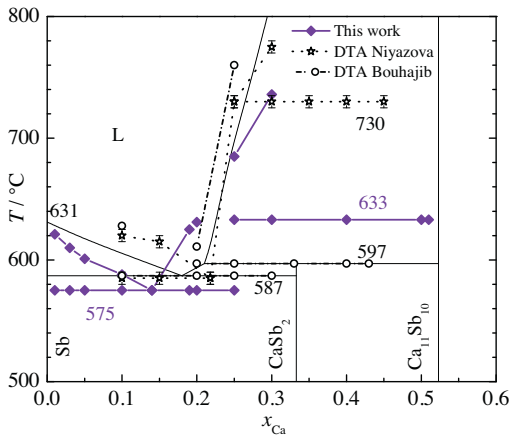

Fig. 6. Liquidus and transition temperatures from emf and DTA measurements [13,3] on Ca–Sb phase diagram [12] (data in Table 4).

temperature at which these fits intersect, the temperature of the phase change can be estimated. The use of intersection points minimized the impact of metastable states on the results. The uncertainty in our temperature evaluation comes from the temperature variation between the different wells, which was measured to be ±2 °C. Also, the emf was not measured continuously with temperature, but only every 20 °C. In Fig. 6, the results are plotted on the latest version of the Ca–Sb phase diagram [12], together with the differential thermal analysis (DTA) measurements by Niyazova et al. [13] and Bouhajib et al. [3]. The intersection points are reported in Table 4.

The overall shape is consistent with the Ca–Sb phase diagram from Okamoto [12], even though the temperature of the L + Sb liquidus is lower than the previous measurements. This might be due to the low number of points available for the L + Sb curve fitting. The peritectic temperature (633 °C ± 12 °C) is between the inconsistent temperatures measured by Niyazova (730 °C ± 5 °C) and Bouhajib (597 °C). This study suggests that the eutectic point occurs at lower Ca content (x_{Ca} = 0.14 vs. 0.18) than reported in [12], although the eutectic temperature is fairly consistent.

4. Thermodynamic modeling of Ca–Sb liquid alloys at 800 °C

Ca–Sb liquid alloys exhibit thermodynamic properties far from ideality. The association model, introduced by Bhatia in 1974 [14], has been used to describe the short-range ordering of liquid alloys such as Na–Sn [8] and Na–Pb [15], systems that form multiple intermetallics in the solid state and have a high-melting intermetallic. One drawback of the association model is the requirement to assume the presence and identity of the associate(s).

A second model that explains the structure of multicomponent liquids is the MIVM introduced by Tao [7]. He used this model successfully for liquid alloys of similar elements, such as Bi, Cd, Pb, Sn, Zn [16]. By describing the melt using a canonical ensemble, this model can take into account the asymmetry of the Ca–Sb interaction without the a priori introduction of an associate. To the authors' knowledge, this model has never been used for liquid alloys of such dissimilar elements.

With Ca–Sb as the physical system of interest, the objective is to reconcile these two models and to show how the structure of liquid Ca–Sb alloys impacts its thermodynamic properties at 800 °C.

Table 4
Liquidus temperatures of Ca–Sb alloys found by intersecting the emf fitting lines.

x_{Ca}	T_{liq} (°C)
0.01	621
0.03	610
0.05	601
0.10	588
0.14	575
0.19	625
0.20	631
0.25	685
0.30	736

4.1. Association model

The association model assumes the formation of associates: $aA + bB = A_aB_b \equiv C$. The liquid alloy is therefore treated as though it is composed of a molecular species C in equilibrium with monoatomic species A and B.

4.1.1. First assumption: composition of associate

The associate(s) usually corresponds to one or several of the intermetallics, i.e. stoichiometric line compounds. The stoichiometry of the associate can be inferred from a peak in the electrical resistivity [17], the shape of the structure factor [18], or a minimum of the entropy of mixing [19]. From the chemical equilibrium of the association reaction, the composition of the ternary melt can be determined:

$$K = \exp\left(-\frac{\Delta H^0 - T\Delta S^0}{RT}\right) = \frac{a_C}{a_A^a a_B^b} = \frac{X_C\gamma_C}{(X_A\gamma_A)^a(X_B\gamma_B)^b} \quad (10)$$

$$X_A = \frac{x - aN_C}{N_T} \quad (11)$$

$$X_B = \frac{1 - x - bN_C}{N_T} \quad (12)$$

$$X_C = \frac{N_C}{N_T} \quad (13)$$

where K is the equilibrium constant of the association reaction, N_C is the number of associates per mole of alloy, $N_T = 1 - (a + b - 1)N_C$ is the number of "particles" (free atoms or associates) per mole of alloy. ΔH^0 and ΔS^0 are the enthalpy and entropy of formation of the associate respectively, x is the fraction of A in the binary alloy, X_i is the fraction of the species i in the ternary melt. The notations used here are the same as those used by Bergman et al. [20].

4.1.2. Second assumption: configurational entropy

The free atoms and associates are located on lattice sites. The first expression for the configurational entropy, s_I, used by Sommer and coworkers [6], assumes that the free atoms and the associates all have the same volume (each species occupies one lattice site only) and are randomly distributed. Other expressions recognize the difference in volume by stating that the associate A_aB_b occupies $a + b$ lattice sites. The Flory expression, s_{II}, takes this difference in volume into account and assumes that the A and B atoms involved in C can be exchanged with free A and B atoms. The third expression, s_{III}, proposed by Bergman in 1982 [20], also takes this difference in volume into account, but describes the structure of the alloy as a quasi-lattice with frozen sites on which monatomic species cannot be exchanged with heteroatomic species. These different expressions for the configurational entropy are:

$$s_I = -R\sum_{i=A,B,C} X_i \ln X_i \quad (14)$$

$$s_{II} = -R\sum_{i=A,B,C} X_i \ln \Phi_i \quad (15)$$

where

$$\Phi_A = \frac{X_A}{X_A + X_B + (a+b)X_C}$$

$$\Phi_B = \frac{X_B}{X_A + X_B + (a+b)X_C}$$

$$\Phi_C = \frac{(a+b)X_C}{X_A + X_B + (a+b)X_C}$$

$$s_{III} = -R\left(\sum_{i=A,B,C} X_i \ln X_i + \ln N_T\right) - R\frac{N_C}{N_T}\ln(a+b) + R\frac{(a+b-1)(1-(a+b)N_C)}{(a+b)N_T}\ln(1-(a+b)N_C) \quad (16)$$

The entropy of mixing is then defined as $\Delta S = N_C \Delta S^0 + N_T s_i$.

4.1.3. Third assumption: interaction model

Depending on the degree of interaction between the monoatomic species and the associate, an interaction model is chosen. In most cases, the regular solution model is sufficient. The enthalpy of mixing is then defined as $\Delta H = N_C \Delta H^0 + N_T \sum_{i \neq j}(\omega_{ij} X_i X_j)$, where ω_{ij} is the interaction coefficient between species i and j.

4.1.4. Application of the regular associated solution model to Ca–Sb liquid alloys

The regular associated solution model was used to model the interaction between the monoatomic species and the associate. The equations introduce 5 parameters: 3 interaction coefficients plus the entropy and the enthalpy of formation of the associate C. These were optimized simultaneously by fitting the thermodynamic properties of mixing ΔH, ΔG, and ΔS. Depending on the starting values chosen, a different solution set can be found for those parameters due to the complexity of the equations, as has been observed by Krull et al. [6]. Following the work of Bouhajib et al. [5], the first associate considered in this work was CaSb. However, the simultaneous fit of the entropy and enthalpy of mixing poorly modeled our experimental data. The associate $CaSb_2$, corresponding to the intermetallic with the highest antimony to calcium ratio, was next tried, and much more satisfactory results were achieved.

The optimized values for each of the configurational entropy expressions are presented in Table 5. The results for ΔH and ΔS after optimization are presented in Fig. 7 in comparison with our experimental values. ΔS modeled using s_I and s_{II} reproduce the shape of the experimental data, and in particular its maximum, more accurately. This implies that the hypothesis made for s_{III}, namely that free Ca and Sb cannot be exchanged with atoms involved in the formation of $CaSb_2$, is not valid for Ca–Sb liquid alloys. Fig. 8 shows that Ca atoms do not exist free in the melt but are associated with Sb forming $CaSb_2$.

4.2. Molecular interaction volume model (MIVM)

Tao proposed the MIVM in 2000 [7] based on the thermodynamic description of a liquid alloy by a canonical ensemble. The energy of each atom depends on a mixing potential energy, which is a function of the identities of the nearest neighbors and their interaction energy with the central atom. Therefore, for an $i-j$ binary alloy, the model can differentiate the energy of an i atom next to a j atom from the energy of a j atom next to an i atom, leading to a non-random distribution of the atoms in the liquid alloy and short-range ordering. This view at the atomic level is different from the macroscopic view of an association model where the interaction between the species is considered with a global $i-j$ interaction coefficient, and the i and j atoms are assumed to be non-randomly distributed in the liquid alloy as associates.

From these new expressions for the configurational partition functions of liquids and their mixtures, Tao expressed the activity coefficients of each of the species i and j in a binary liquid alloy $i-j$

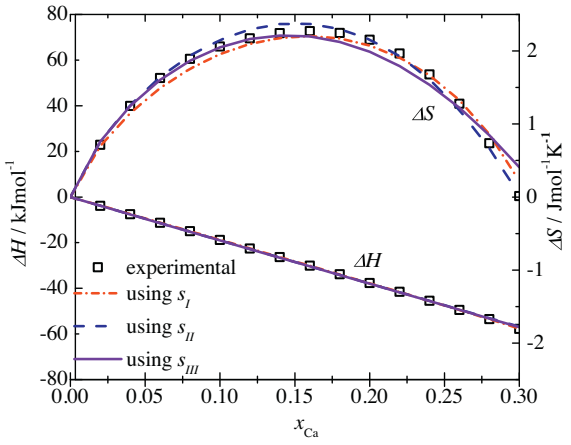

Fig. 7. Enthalpy and entropy of mixing of Ca–Sb liquid alloys vs. Ca concentration at 800 °C.

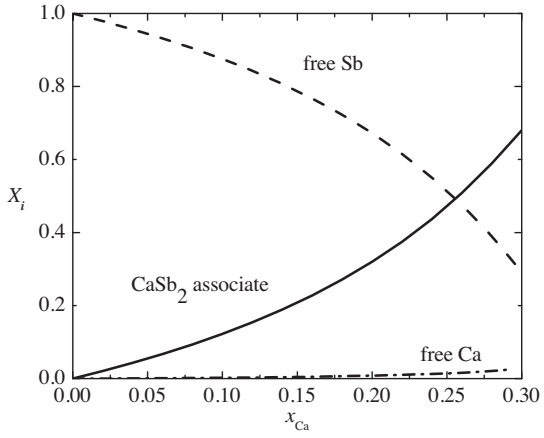

Fig. 8. Composition of the ternary melt at 800 °C using s_{II}.

Table 5
Enthalpy and entropy of formation of $CaSb_2$ and of the interaction coefficients found for each expression of the configurational entropy at 800 °C.

	ΔH^0 (kJ/mol)	ΔS^0 (J/mol/K)	ω_{Ca-Sb} (kJ/mol)	$\omega_{Ca-CaSb_2}$ (kJ/mol)	$\omega_{Sb-CaSb_2}$ (kJ/mol)
With s_I	−194 ± 1	−5.5 ± 0.1	−10.5 ± 1	−28 ± 1	7.5 ± 1
With s_{II}	−192 ± 1	−10.1 ± 0.1	−138 ± 1	−136.5 ± 1	1.5 ± 1
With s_{III}	−190 ± 1	−2 ± 0.1	−195 ± 1	−113 ± 1	−2 ± 1

Table 6
Input parameters in the MIVM: molar volume and atomic first coordination number.

Element	V_m (m^3/ mol) [21]	Z [22]
Ca at 842 °C	29.54×10^{-6}	10.33
Sb at 800 °C	19.21×10^{-6}	8.53
Sb at 650 °C	18.85×10^{-6}	8.70

[7]. The notations used here are those of Tao:

$$\ln \gamma_i = \ln\left(\frac{V_{mi}}{x_i V_{mi} + x_j V_{mj} B_{ji}}\right) + x_j\left(\frac{V_{mj}B_{ji}}{x_i V_{mi} + x_j V_{mj} B_{ji}} - \frac{V_{mi}B_{ij}}{x_j V_{mj} + x_i V_{mi} B_{ij}}\right) - \frac{x_j^2}{2}\left(\frac{Z_i B_{ji}^2 \ln B_{ji}}{(x_i + x_j B_{ji})^2} + \frac{Z_j B_{ij} \ln B_{ij}}{(x_j + x_i B_{ij})^2}\right) \quad (17)$$

$$\ln \gamma_j = \ln\left(\frac{V_{mj}}{x_j V_{mj} + x_i V_{mi} B_{ij}}\right) + x_i\left(\frac{V_{mi}B_{ij}}{x_j V_{mj} + x_i V_{mi} B_{ij}} - \frac{V_{mj}B_{ji}}{x_i V_{mi} + x_j V_{mj} B_{ji}}\right) - \frac{x_i^2}{2}\left(\frac{Z_j B_{ij}^2 \ln B_{ij}}{(x_j + x_i B_{ij})^2} + \frac{Z_i B_{ji} \ln B_{ji}}{(x_i + x_j B_{ji})^2}\right) \quad (18)$$

where V_m is the molar volume, Z is the atomic first coordination number, and B_{ji} and B_{ij} the pair potential interaction parameters. $B_{ji} = \exp(-(\epsilon_{ji} - \epsilon_{ii})/kT)$, where ϵ_{ii} is the $i-i$ pair potential energies and $\epsilon_{ij} = -kT\ln(Z_{ij}/x_j)$, where Z_{ij} is the number of j atoms surrounding the central i atom. B_{ij} is defined similarly. The values used for the input parameters V_m and Z are reported in Table 6. For Ca, the properties at its melting point were used even though the temperature of analysis is below the melting point of Ca.

To solve Eqs. (17) and (18) for B_{ji} and B_{ij}, Tao uses the values of the activity coefficients at infinite dilution, which simplifies the equations [16]. Here, B_{ji} and B_{ij} were found by fitting the full equations to our experimental a_{Ca}. Only a_{Ca} was considered as a_{Sb} was not measured independently. Since a_{Ca} was obtained by emf measurements, the parameter optimized in the present algorithm is $|E_{calc} - E_{measured}|^2$, where a_{Ca} is related to E by Eq. (3).

The interaction parameters found are $B_{Sb-Ca} = 23.93$ and $B_{Ca-Sb} = 1.16$. The average difference between the emf predicted and the emf measured was 5.7 mV, or 0.5% of the emf measured (Table 7, Fig. 9).

In the case of alloys with similar elements [7], Tao found interaction parameters close to 1. To interpret this difference, the fractions of Ca and Sb surrounding Ca and Sb are presented in Fig. 10. While the fractions of Ca and Sb surrounding Sb correspond to random mixing, as in the alloys studied by Tao, Ca atoms are surrounded almost exclusively by Sb atoms.

Table 7
Experimental and predicted activities of Ca in Ca–Sb alloys at 800 °C and corresponding emf difference.

x_{Ca}	a_{Ca} exp	a_{Ca} model	Emf error (mV)
0.01	8.15×10^{-12}	1.14×10^{-11}	−15.6
0.03	3.65×10^{-11}	3.95×10^{-11}	−3.6
0.05	8.97×10^{-11}	7.57×10^{-11}	7.9
0.10	2.46×10^{-10}	2.13×10^{-10}	6.6
0.14	3.90×10^{-10}	3.92×10^{-10}	−0.2
0.19	7.41×10^{-10}	7.46×10^{-10}	−0.3
0.20	8.16×10^{-10}	8.39×10^{-10}	−1.3
0.25	1.35×10^{-9}	1.47×10^{-9}	−4.0
0.30	1.93×10^{-9}	2.49×10^{-9}	−11.8

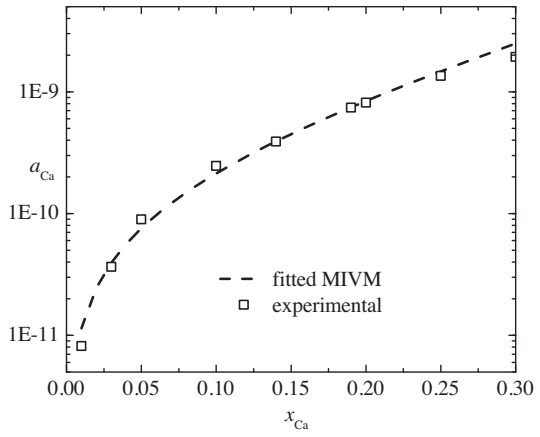

Fig. 9. Activity of Ca vs. Ca concentration in Ca–Sb liquid alloys at 800 °C.

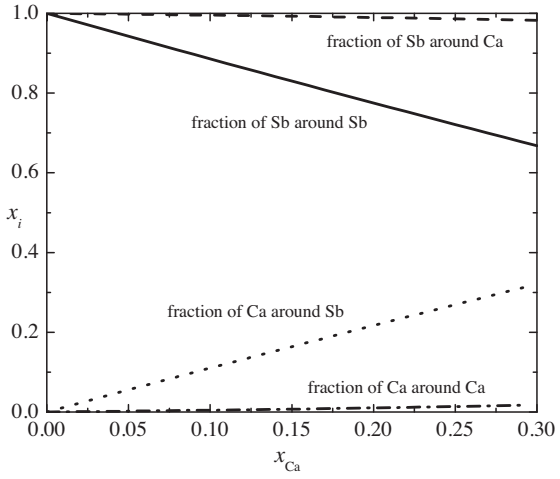

Fig. 10. The variation of Ca and Sb environments vs. Ca concentration in Ca–Sb liquid alloys at 800 °C.

4.3. Comparison of the association model and the MIVM

Both models show that Ca–Sb liquid alloys do not exhibit random mixing but rather short-range ordering. In the association model, the formation of $CaSb_2$ associates explains the shape of the thermodynamic properties of mixing of the Ca–Sb alloys. In this case, Ca does not exist as a free atom in the ternary melt, but is stabilized when associated with Sb to form $CaSb_2$. Since $CaSb_2$ and Sb are the two species present in the melt, the Ca atoms forming $CaSb_2$ associates are almost exclusively surrounded by Sb atoms. The MIVM gives a different perspective of the same phenomenon by considering the first nearest neighbors of Ca and Sb and showing that Ca atoms are almost exclusively surrounded by Sb. In the case of Ca–Sb liquid alloys, the association model and the MIVM can therefore be reconciled.

4.4. Prediction of the activity coefficients of Ca at 650 °C using the MIVM

Herein, the MIVM has been shown to be a viable alternative to the regular associated model for the analysis of liquid alloys systems with high-melting intermetallics, reducing the number of fitting parameters necessary from 5 (regular associated model) to

Table 8
Experimental and predicted activities of Ca in Ca–Sb alloys at 650 °C and corresponding emf difference.

x_{Ca}	a_{Ca} exp	a_{Ca} predicted	Emf error (mV)
0.01	3.00×10^{-13}	4.04×10^{-13}	−13.8
0.03	1.44×10^{-12}	1.40×10^{-12}	1.5
0.05	3.55×10^{-12}	2.69×10^{-12}	12.9
0.10	9.19×10^{-12}	7.60×10^{-12}	8.8
0.14	1.46×10^{-11}	1.39×10^{-11}	2.2
0.19	2.75×10^{-11}	2.63×10^{-11}	2.0
0.20	2.96×10^{-11}	2.96×10^{-11}	0.0

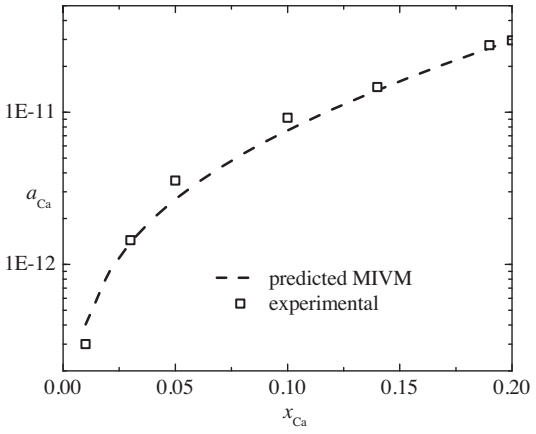

Fig. 11. Activity of Ca vs. Ca concentration in Ca–Sb liquid alloys at 650 °C.

2 (MIVM). The temperature dependence of the interaction coefficients derived by Tao, $B_{ji} = \exp(-(\epsilon_{ji} - \epsilon_{ii})/kT)$ assuming a constant $\epsilon_{ji} - \epsilon_{ii}$, allows one to predict the interaction coefficients of Ca–Sb liquid alloys at different temperatures.

The interaction parameters at 650 °C calculated from the temperature dependence are $B_{Sb-Ca} = 40.09$ and $B_{Ca-Sb} = 1.19$. The variation of V_m and Z was taken into account for Sb, using the values at 650 °C from Table 6, whereas the properties at its melting point were again used for Ca. The calculation of a_{Ca} using these parameters gave an average difference between the emf predicted and the emf measured of 5.9 mV, or 0.6% of the absolute emf value (Table 8, Fig. 11).

For the alloys considered by Tao, the values of the interaction coefficients never deviated much from unity, and therefore almost no temperature dependence was observed. In contrast, for the Ca–Sb alloys of the present study, the values of B_{Sb-Ca} exhibited significant variation with temperature and yet the MIVM accurately represents the quantitative nature of this variation.

5. Conclusion

The activity coefficient of Ca in Ca–Sb liquid alloys was measured by emf measurements and found to vary between 8×10^{-12} and 2×10^{-9} at 800 °C and between 3×10^{-13} and 3×10^{-11} at 650 °C. Based on these results, we judge Sb to be an attractive choice for the positive electrode of a Ca-based liquid metal battery as the voltage remains high (close to 1V) and the electrode does not completely solidify over a wide range of concentration ($0 < x_{Ca} < 0.5$). The melting points of Ca–Sb alloys between $x_{Ca} = 0.01$ and $x_{Ca} = 0.25$ were estimated by intersecting the fitted emf vs. temperature lines, questioning in particular the peritectic temperature of the currently accepted phase diagram.

For the first time, the MIVM was used successfully to model the thermodynamic properties of liquid alloys in a system with high-melting intermetallics without making assumptions about the presence of an associate and decreasing the number of fit parameters from 5 to 2, offering an alternative to the commonly used regular associated model.

Acknowledgments

The authors acknowledge the invaluable assistance of Alex Zevalkink of the Dr. G. J. Snyder group at Caltech in the preparation of the powder processed samples, Dr. D.A. Boysen for his fruitful discussions and advice, and TOTAL S.A. and the US Department of Energy, Advanced Research Projects Agency – Energy (Award No. DE-AR000047) for their financial support.

References

[1] D. Bradwell, G. Ceder, L. Ortiz, D. Sadoway, Liquid electrode battery, US Patent Appl. 12/839,130 (2010).
[2] D.J. Bradwell, H. Kim, A.H.C. Sirk, D.R. Sadoway, Magnesium-antimony liquid metal battery for stationary energy storage, Journal of the American Chemical Society 134 (4) (2012) 1895–1897.
[3] A. Bouhajib, M. Notin, A. Nadiri, A. Yacoubi, Calorimetric study coupled with a numerical optimization technique for the Ca–Sb system, High Temperature Materials and Processes 18 (1999) 151.
[4] M. Notin, J. Mejbar, A. Bouhajib, J. Charles, J. Hertz, The thermodynamic properties of calcium intermetallic compounds, Journal of Alloys and Compounds (Switzerland) 220 (1995) 62.
[5] A. Bouhajib, A. Nadiri, A. Yacoubi, R. Castanet, Investigation of the short-range order in the Ca–Sb melts, Journal of Alloys and Compounds (Switzerland) 287 (1999) 167.
[6] H.-G. Krull, R. Singh, F. Sommer, Generalised association model, Zeitschrift fur Metallkunde (Germany) 91 (2000) 356.
[7] D.P. Tao, A new model of thermodynamics of liquid mixtures and its application to liquid alloys, Thermochimica Acta 363 (2000) 105.
[8] S. Tamaki, T. Ishiguro, S. Takeda, Thermodynamic properties of liquid Na–Sn alloys, Journal of Physics F – Metal Physics 12 (1982) 1613.
[9] A. Petric, A. Pelton, M.-L. Saboungi, Thermodynamic properties of liquid K–Bi alloys by electromotive force measurements, Journal of Physics F – Metal Physics 18 (1988) 1473.
[10] H. Kim, D. Boysen, D.J. Bradwell, B. Chung, K. Jiang, A.A. Tomaszowska, K. Wang, W. Wei, D.R. Sadoway, Thermodynamic properties of calcium–bismuth alloys determined by emf measurements, Electrochimica Acta 60 (2012) 154.
[11] A. Zevalkink, E.S. Toberer, W.G. Zeier, E. Flage-Larsen, G.J. Snyder, Ca_3AlSb_3: an inexpensive, non-toxic thermoelectric material for waste heat recovery, Energy and Environmental Science 4 (2011) 510.
[12] H. Okamoto, Ca–Sb (calcium–antimony), Journal of Phase Equilibria 18 (1997) 313.
[13] Z. Niyazova, A. Vakhobov, T. Dzhuraev, Phase diagram of the system Ca–Sb, Inorganic Materials (USA) 12 (1976) 1074.
[14] A. Bhatia, W. Hargrove, Concentration fluctuations and thermodynamic properties of some compound forming binary molten systems, Physical Review B 10 (1974) 3186.
[15] S. Matsunaga, T. Ishiguro, S. Tamaki, Thermodynamic properties of liquid Na–Pb alloys, Journal of Physics F – Metal Physics (UK) 13 (1983) 587.
[16] D.P. Tao, Prediction of the thermodynamic properties of multicomponent liquid alloys by binary infinite dilute activity coefficients, Metallurgical and Materials Transactions B: Process Metallurgy and Materials Processing Science 32 (2001) 1205.
[17] A. Rais, N. Cusak, F. Neale, Simultaneous measurement of resistivity and thermodynamic properties of liquid binary alloys. application to Na–In, Na–Sn, Journal of Physics F – Metal Physics (UK) 12 (1982) 1091.
[18] B. Alblas, W. van der Lugt, J. Dijkstra, W. Geertsma, C. van Dijk, Structure of liquid Na–Sn alloys, Journal of Physics F – Metal Physics (UK) 13 (1983) 2465.
[19] S. Tamaki, N. Cusack, Thermodynamic properties of liquid Na–Ga alloys, Journal of Physics F – Metal Physics (UK) 9 (1979) 403.
[20] C. Bergman, R. Castanet, H. Said, M. Gilbert, J.-C. Mathieu, Configurational entropy and the regular associated model for compound-forming binary systems in the liquid state, Journal of the Less-Common Metals (Switzerland) 85 (1982) 121.
[21] T. Iida, R.I. Guthrie, The Physical Properties of Liquid Metals, Clarendon Press, Oxford, 1988.
[22] D.P. Tao, Prediction of the coordination numbers of liquid metals, Metallurgical and Materials Transactions A – Physical Metallurgy and Materials Science (USA) 36A (2005) 3495.